Cooperative effects in dense cold atomic gases including magnetic dipole interactions

N. S. Baßler,[1,2] I. Varma,[3] M. Proske,[3] P. Windpassinger,[3] K. P. Schmidt,[1] and C. Genes[1,2]
[1]*Department of Physics, Friedrich-Alexander Universität Erlangen-Nürnberg (FAU), Staudtstraße 7, D-91058 Erlangen, Germany*
[2]*Max Planck Institute for the Science of Light, Staudtstraße 2, D-91058 Erlangen, Germany*
[3]*Institut für Physik, Johannes Gutenberg-Universität Mainz, 55122 Mainz, Germany*

(Received 13 July 2023; accepted 22 April 2024; published 9 May 2024)

We theoretically investigate cooperative effects in cold atomic gases exhibiting both electric and magnetic dipole-dipole interactions, such as occurs, for example, in clouds of dysprosium atoms. After introducing a general framework capturing both the quantum degenerate and nondenegerate cases, we focus on the emergence of tailorable spin models in the quantum nondegenerate regime. In the low-excitation limit, we provide analytical and numerical results detailing the effect of magnetic interactions on the directionality of scattered light and characterize sub and superradiant effects.

DOI: 10.1103/PhysRevResearch.6.023147

I. INTRODUCTION

Scattering of light off atomic gases necessarily involves aspects of quantum cooperativity, arising from the common, hybrid reaction of closely positioned and mutually coupled quantum emitters to the external stimulation [1]. The optical response can be very complex, as it strongly depends on the gas density and temperature, the type of atoms comprising the gas, as well as on the strength of the driving field. For low density and high temperature, an independent scattering regime can be obtained where the gas response can be deduced from the single atom response [2,3]. For higher density, weak excitation, and still high temperature, cooperative aspects such as super [4,5] and subradiance [6] (spontaneous emission rates larger or smaller than that of an isolated particle) emerge. Many features of such ensembles have already been investigated theoretically and experimentally [7]. A dense ensemble exhibits a cooperative lineshift [8–10] that cannot be predicted from standard electrodynamics of a dielectric [11]. Superradiant emission is directional [12] and robust to many perturbations of the system [13]. The superradiant level structure is, however, completely quantum mechanical [14] and not simply due to synchronization of dipoles as proven by single-photon superradiance experiments [15,16]. There exist promising applications of superradiant ensembles such as the generation of pulse trains using the burst [17]. There are also investigations into the consequences of additional effects such as more complex level structures and atomic motion in different regimes [18,19]. The results for some dense cloud experiments are, however, still not in complete agreement with theory [20]. High driving powers lead then to nonlinear optical effects [21], as the atomic transitions can saturate and atoms become fundamentally nonlinear elements.

In all cases discussed so far, a simple quantum optics approach suffices, based on the open quantum system formalism, where most of the relevant features and behaviors are obtained in a two-level system approach where atoms are treated as pseudospins 1/2 (with transitions between ground and excited electronic orbitals) responding to an external stimulation.

In the low-temperature limit, the motional wavepackets of the atoms comprising the gas can overlap, leading to a change in the theoretical framework, which must necessarily include a many-body formulation to the problem [22–25]. This is illustrated in Fig. 1 where the nonoverlapping motional wavepackets case corresponding to a thermal, classical gas is shown in Fig. 1(b) while the quantum degenerate limit involving overlapping wave functions is depicted in Fig. 1(c). The quantum degenerate gas has been shown theoretically [26] and experimentally [8–10] to lead to fermionic subradiance via Pauli blocking [27–29] and to superradiance in Bose-Einstein condensates [30,31].

We introduce here analytical tools to describe both the quantum nondegenerate and quantum degenerate cases, however, with a focus on the first of these. To this end we extend the formulation of the cooperative response to include magnetic interactions on top of the standard electric dipole-dipole exchanges, as, for example, strongly present in experiments with dysprosium atoms [32,33]. In the arbitrarily strong drive limit, for classical gases, we show the emergence of a spin Hamiltonian with tunable parameters. In the weak driving limit, a simpler coupled dipoles approach suffices. This can be seen also as a reduction of the dynamics onto the bottom of the Bloch sphere involving only single excitation collective states. The results show slight modifications in the superradiant response.

The paper is organized as follows. In Sec. II we introduce the light-matter interaction model at the Hamiltonian level for both degenerate (Sec. II B) and nondegenerate gases

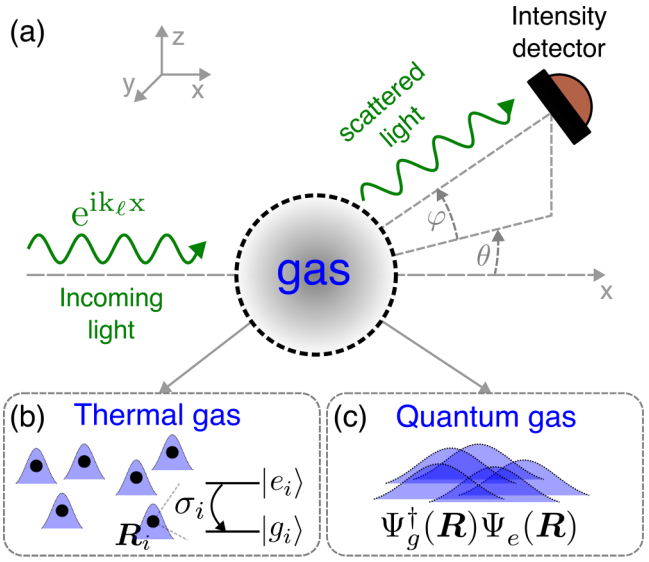

FIG. 1. (a) Schematics of the system. (b) In the first case, the de Broglie wavelength of each atom is much smaller than the average interparticle separation, allowing one to treat the system as a classical thermal gas far from quantum degeneracy. (c) In the opposite limit, quantum degeneracy is achieved by lowering the temperature and consequently producing particles with overlapping de Broglie wavepackets. To compute the optical response, a quantum many-body approach to the problem is necessary.

(Sec. II A) including both electric and magnetic dipole-dipole interactions. In Sec. III we reduce our treatment to the nondegenerate case, where we first analyze the strong driving limit and show the emergence of a many-particle spin Hamiltonian with interactions of tunable strength. We then exemplify the magnetic dipole interactions effect on the light scattered in the weak driving regime and find small deviations from a purely electrically interacting gas.

II. MODEL

We consider $\mathcal{N}$ atoms (positioned at $\boldsymbol{R}_i$ with index i running from 1 to $\mathcal{N}$) trapped in an external potential (see Table I for a list of notation used in this article). Optical addressing of each atom (both by classical fields and the quantum electromagnetic vacuum modes) is achieved by coupling to its single valence electron, which we denote by its position $\boldsymbol{r}_i$ measured with respect to the position of the nucleus. The atomic cloud is illuminated by a laser with Rabi frequency Ω, wave vector k_ℓ, and frequency $\omega_\ell = ck_\ell$ propagating in the x direction as depicted in Fig. 1(a). Two distinct regimes emerge: (i) a *quantum nondegenerate limit* where atomic motion is described by a thermal distribution of velocities and (ii) a *quantum degenerate limit* where atomic motion is quantized and atoms become indistinguishable, thus the quantum degenerate case. The distinction between the two cases is illustrated in Figs. 1(b) and 1(c) where the overlap of individual atomic de Broglie wavepackets indicates the criterion for the transition between the two limits. In both cases, we will be interested in the spectroscopic quantities obtained from a detector positioned in the far-field regime with angles θ and ϕ with respect to the incoming laser.

TABLE I. Table of definitions.

Quantity	Definition
$\Gamma(\Gamma_\mu)$	Electric (magnetic) radiative loss rate
f_{ij}^d	Dissipative electric dipole interaction
g_{ij}^d	Coherent electric dipole interaction
$\Omega_{i,j}^{\alpha,\beta}$	Static magnetic dipolar interaction
$\eta_{n,m}$	Franck-Condon factors
$\boldsymbol{k}_\ell$	Laser wave vector
k_ℓ	Laser wave vector magnitude
ω_ℓ	Laser frequency
ω_0	Transition frequency
Δ	Laser detuning
g_k	Photon coupling strength
$\epsilon_{\boldsymbol{k}}$	Photon polarization vector
$\hat{\boldsymbol{d}}_i$	Electric transition dipole operator
$\hat{\boldsymbol{\mu}}_i$	Magnetic transition dipole operator
$\hat{\boldsymbol{\mu}}_{s,i}$	Magnetic static dipole operator
$\boldsymbol{d}_i$	Electric transition dipole moment
$\boldsymbol{\mu}_i$	Magnetic transition dipole moment
$\boldsymbol{\mu}_{i,e}$	Static magnetic dipole moment of excited state
$\boldsymbol{\mu}_{i,g}$	Static magnetic dipole moment of ground state
σ_i	Transition operator
σ_i^z	Inversion operator
$\hat{a}_{\boldsymbol{k},\boldsymbol{\epsilon}}$	Photon annihilation operator
$\hat{\boldsymbol{r}}_i$	Relative electron position of transition
$\hat{\boldsymbol{L}}_i$	Angular momentum operator
$\hat{\boldsymbol{E}}(\boldsymbol{R})$, $(\hat{\boldsymbol{B}}(\boldsymbol{R}))$	Electric (magnetic) field operator at position $\boldsymbol{R}$
$\Psi_g(\boldsymbol{R})$	Annihilation operator for ground state atom at $\boldsymbol{R}$
$\Psi_e(\boldsymbol{R})$	Annihilation operator for excited state atom at $\boldsymbol{R}$
$\boldsymbol{v}_{\text{drive}}$	Drive vector for small drive
$\mathcal{M}$	Interaction matrix for small drive
$\delta\omega_j$	Frequency shift due to static magnetic field
μ_e	Excited state magnetic moment
μ_g	Ground state magnetic moment
Ω_μ	Magnetic interaction frequency
$\boldsymbol{r}_s$	Detector position
$\boldsymbol{k}_s$	Detector wave vector
$\mathcal{N}_c$	Number of runs over configurations
$\mathcal{N}$	Number of total atoms
τ	Optical depth
θ	Detection angle
$\hat{\Sigma}(\boldsymbol{R})$	Transition operator acting at position $\boldsymbol{R}$
$\hat{e}_{\boldsymbol{m}}$	Annihilation operator for excited state $\boldsymbol{m}$
$\hat{g}_{\boldsymbol{m}}$	Annihilation operator for ground state $\boldsymbol{m}$
$\Sigma_{\boldsymbol{n},\boldsymbol{m}}$	Transition operator between $\boldsymbol{n}$ and $\boldsymbol{m}$
$\mathcal{N}_g$	Number of atoms in the ground state
$\mathcal{N}_e$	Number of atoms in the excited state
$I(\boldsymbol{k}_s)$	Intensity at detection vector $\boldsymbol{k}_s$
$\omega_{\boldsymbol{n}}$	Frequency of state $\boldsymbol{n}$
$\boldsymbol{R}_i$	Center of mass position of atom i

For simplicity of presentation, we proceed with a set of approximations which are usually performed in treating light-matter interactions. We perform the dipole approximation which assumes that the size of the electronic orbital is negligible with respect to any relevant optical transition wavelength λ. In addition, we assume nonoverlapping electronic orbitals between neighboring atoms. The electric and

magnetic fields are quantized in a fictitious box of volume $\mathcal{V}$ and expressed in terms of photon creation and annihilation bosonic operators $\hat{a}_{\boldsymbol{k},\boldsymbol{\epsilon}}$ with frequencies $\omega_k = c|\boldsymbol{k}|$ and commutators $[\hat{a}_{\boldsymbol{k},\boldsymbol{\epsilon}_k}, \hat{a}^\dagger_{\boldsymbol{k}',\boldsymbol{\epsilon}'_k}] = \delta_{\boldsymbol{k},\boldsymbol{k}'}\delta_{\boldsymbol{\epsilon}_k,\boldsymbol{\epsilon}'_k}$ (where $\boldsymbol{\epsilon}_k$ is the polarization for the mode $\boldsymbol{k}$). The free-space quantization yields the electric and magnetic field operators

$$\hat{\boldsymbol{E}} = \mathrm{i}\sum_{\boldsymbol{k},\boldsymbol{\epsilon}} g_k \omega_k \boldsymbol{\epsilon}_{\boldsymbol{k}} (\hat{a}_{\boldsymbol{k},\boldsymbol{\epsilon}} e^{\mathrm{i}\boldsymbol{k}\boldsymbol{R}} - \hat{a}^\dagger_{\boldsymbol{k},\boldsymbol{\epsilon}} e^{-\mathrm{i}\boldsymbol{k}\boldsymbol{R}}), \tag{1}$$

$$\hat{\boldsymbol{B}} = \mathrm{i}\sum_{\boldsymbol{k},\boldsymbol{\epsilon}} (\boldsymbol{k}\times\boldsymbol{\epsilon}_{\boldsymbol{k}}) g_k (\hat{a}_{\boldsymbol{k},\boldsymbol{\epsilon}} e^{\mathrm{i}\boldsymbol{k}\boldsymbol{R}} - \hat{a}^\dagger_{\boldsymbol{k},\boldsymbol{\epsilon}} e^{-\mathrm{i}\boldsymbol{k}\boldsymbol{R}}), \tag{2}$$

with $g_k = 1/\sqrt{2\omega_k \mathcal{V}\epsilon_0}$ being the photon coupling strength. From here on the treatment is distinct for the two assumed limits of either a gas with a classical distribution of velocities or a quantum degenerate gas of indistinguishable atoms.

A. Quantum nondegenerate gas approach

We follow the standard quantum optics approach where the internal electronic dynamics of each atom is treated in terms of Pauli matrices. To this end, we restrict the dynamics of the electron to a ground state $|g\rangle_i$ and a single excited state $|e\rangle_i$, separated by frequency ω. Notice that, in practice, this assumption is a very good approximation for optically pumped atoms. An example based on dysprosium atoms is shown in Appendix A where the ground state is represented by a magnetic sublevel with $J = 8$ and $m_J = -8$ and the excited state with $J' = 9$ and $m'_J = -9$.

The Pauli matrices represent transitions in the electronic degrees of freedom and are defined as $\sigma_i = |g\rangle_i\langle e|_i$. The coupling to electromagnetic waves occurs via either the transition electric $\hat{\boldsymbol{d}}_i = \boldsymbol{d}_i\sigma_i + \boldsymbol{d}_i^*\sigma_i^\dagger$ and magnetic $\hat{\boldsymbol{\mu}}_i = \boldsymbol{\mu}_i\sigma_i + \boldsymbol{\mu}_i^*\sigma_i^\dagger$ dipole operators or via the static magnetic dipole operator $\hat{\boldsymbol{\mu}}_{s,i} = \boldsymbol{\mu}_{i,e}\sigma_i^\dagger\sigma_i + \boldsymbol{\mu}_{i,g}\sigma_i\sigma_i^\dagger$. The static components of the magnetic dipole $\boldsymbol{\mu}_{i,e}$ and $\boldsymbol{\mu}_{i,g}$ are computed within their respective electronic states, as $\boldsymbol{\mu}_{i,e} = -g\mu_B\langle e_i|\hat{\boldsymbol{L}}_i|e_i\rangle$ and $\boldsymbol{\mu}_{i,g} = -g\mu_B\langle g_i|\hat{\boldsymbol{L}}_i|g_i\rangle$. The operator $\hat{L}_i$ is the angular momentum of atom i, μ_B is the Bohr magneton, and g is the Landé factor. The transition dipole matrix elements are computed between orbitals $\boldsymbol{d}_i = -e\langle e_i|\hat{\boldsymbol{r}}_i|g_i\rangle$ and $\boldsymbol{\mu}_i = -g\mu_B\langle g_i|\hat{\boldsymbol{L}}_i|e_i\rangle$. Due to the fixed parity of hydrogen-like orbitals, the static electric dipole moment must vanish, which is not the case for the static magnetic dipole moment. The resulting Hamiltonian

$$\mathcal{H} = \mathcal{H}_{\mathrm{at}} + \mathcal{H}_{\mathrm{em}} + \mathcal{H}_{\mathrm{el+mag}} + \mathcal{H}_{\mathrm{drive}}, \tag{3}$$

is a sum over the free Hamiltonians of the atoms $\mathcal{H}_{\mathrm{at}}$, the electromagnetic vacuum Hamiltonian $\mathcal{H}_{\mathrm{em}}$, the electric and magnetic dipole coupling to the radiation field $\mathcal{H}_{\mathrm{el+mag}}$, and the semiclassical drive $\mathcal{H}_{\mathrm{drive}}$.

The first two terms are explicitly written as

$$\mathcal{H}_{\mathrm{at}} + \mathcal{H}_{\mathrm{em}} = \omega\sum_i \sigma_i^\dagger\sigma_i + \sum_{\boldsymbol{k},\boldsymbol{\epsilon}} \omega_k \hat{a}^\dagger_{\boldsymbol{k},\boldsymbol{\epsilon}_k}\hat{a}_{\boldsymbol{k},\boldsymbol{\epsilon}_k}, \tag{4}$$

where we set the zero of the energy at the ground electronic state level and ignored the zero-point energy of the vacuum modes. The coupling of the atomic system to the electric and magnetic quantum fields is

$$\mathcal{H}_{\mathrm{el+mag}} = \sum_i \hat{\boldsymbol{d}}_i\cdot\hat{\boldsymbol{E}}(\boldsymbol{R}_i) + (\hat{\boldsymbol{\mu}}_{t,i} + \hat{\boldsymbol{\mu}}_{s,i})\cdot\hat{\boldsymbol{B}}(\boldsymbol{R}_i). \tag{5}$$

The semiclassical drive is characterized by the Rabi frequency Ω and is written as

$$\mathcal{H}_{\mathrm{drive}} = \Omega\sum_i (e^{-\mathrm{i}\boldsymbol{k}_\ell\boldsymbol{R}_i}\sigma_i + e^{\mathrm{i}\boldsymbol{k}_\ell\boldsymbol{R}_i}\sigma_i^\dagger), \tag{6}$$

where $\boldsymbol{k}_\ell = k_\ell\hat{e}_x$ and $\hat{e}_x$ is the unit vector in the x-direction. The Hamiltonian above is the starting point for the models analyzed in Sec. III.

B. Quantum degenerate gas approach

In the opposite limit of a quantum degenerate gas, it is more convenient to introduce a two-species model where field operators $\Psi^\dagger_{e,g}(\boldsymbol{R})$ create atoms at some position $\boldsymbol{R}$ with their electron either in the ground or in the excited state. The dipole moments can be written in terms of field operators as the action of the Pauli matrices is now expressed by combinations of the field operators. For example, the operator $\hat{\Sigma}(\boldsymbol{R}) = \Psi^\dagger_g(\boldsymbol{R})\Psi_e(\boldsymbol{R})$ is the field-theoretical equivalent of the matrix operator σ_i where the particle location, which was previously denoted by an index, is now denoted by a continuous variable due to the replacement of localized scatterers by fields. The meaning is that an atom in the excited state is destroyed while another atom in the ground state is created in exactly the same position. The commutation relations are the standard ones $[\Psi_\alpha(\boldsymbol{R}), \Psi^\dagger_\beta(\boldsymbol{R}')]_\zeta = \delta(\boldsymbol{R}-\boldsymbol{R}')\delta_{\alpha,\beta}$, where $\alpha,\beta\in\{e,g\}$ are species indices while ζ specifies commutation or anticommutation relations depending on the bosonic or fermionic nature of the gas. The single-particle motional Hamiltonian is written as

$$\mathcal{H}_0 = -\nabla^2/2M + V_{\mathrm{ext}}(\boldsymbol{R}), \tag{7}$$

where $V_{\mathrm{ext}}(\boldsymbol{R})$ is an externally applied potential (assumed quadratic in the following) that allows for the use of a simpler notation using the trap basis states. Notice that, with a state-independent choice for $V_{\mathrm{ext}}(\boldsymbol{R})$, the motional wave functions are the same for the excited-type and ground-state-type atoms.

In the second quantization, the total system Hamiltonian is obtained as an integration of the Hamiltonian density. As a next step, the field operators can be expanded in a conveniently chosen basis. In particular, we will consider the trap basis defined by the eigenvectors $\mathcal{H}_0\phi_{\boldsymbol{n}} = \omega_{\boldsymbol{n}}\phi_{\boldsymbol{n}}$. Particle creation and annihilation operators can then be defined as

$$\begin{aligned}\hat{g}_{\boldsymbol{n}} &= \int d\boldsymbol{R}[\phi_{\boldsymbol{n}}(\boldsymbol{R})]^*\Psi_g(\boldsymbol{R}),\\ \hat{e}_{\boldsymbol{n}} &= \int d\boldsymbol{R}[\phi_{\boldsymbol{n}}(\boldsymbol{R})]^*\Psi_e(\boldsymbol{R}).\end{aligned} \tag{8}$$

The operators can be interpreted in the following way: when $\hat{g}^\dagger_{\boldsymbol{n}}$ is applied to the vacuum, it creates an atom in the trap state $\boldsymbol{n}$ and in the electronic ground state. Similarly, $\hat{e}^\dagger_{\boldsymbol{n}}$ creates an atom in the trap state $\boldsymbol{n}$ and in the electronic excited state. The fermionic or bosonic nature of the atoms is consistently taken into account by the commutation relations of these operators. The transition from free particles to trapped ones is performed by the tuning of the single-particle trapping potential, which,

in turn, affects the shape of the trap basis eigenvectors. With this, the free Hamiltonian of the atoms can be written as

$$\mathcal{H}_{\rm at} = \sum_{\boldsymbol{n}} \omega_{\boldsymbol{n}} \hat{g}^\dagger_{\boldsymbol{n}} \hat{g}_{\boldsymbol{n}} + \sum_{\boldsymbol{n}} (\omega_0 + \omega_{\boldsymbol{n}}) \hat{e}^\dagger_{\boldsymbol{n}} \hat{e}_{\boldsymbol{n}}. \tag{9}$$

The electromagnetic modes Hamiltonian $\mathcal{H}_{\rm em}$ is the same as before. The coupling of the atomic system to the electric and magnetic quantum fields is described by the following Hamiltonian:

$$\begin{aligned}\mathcal{H}_{\rm el+mag} = &\sum_{\boldsymbol{n},\boldsymbol{m}} (\hat{\Sigma}_{\boldsymbol{n},\boldsymbol{m}} + \hat{\Sigma}^\dagger_{\boldsymbol{n},\boldsymbol{m}}) \langle \boldsymbol{n}|\boldsymbol{d}\cdot\boldsymbol{E}(\boldsymbol{R})|\boldsymbol{m}\rangle \\ &+ \sum_{\boldsymbol{n},\boldsymbol{m}} (\hat{\Sigma}_{\boldsymbol{n},\boldsymbol{m}} + \hat{\Sigma}^\dagger_{\boldsymbol{n},\boldsymbol{m}}) \langle \boldsymbol{n}|\boldsymbol{\mu}\cdot\boldsymbol{B}(\boldsymbol{R})|\boldsymbol{m}\rangle \\ &+ \sum_{\boldsymbol{n},\boldsymbol{m}} (\hat{g}^\dagger_{\boldsymbol{n}} \hat{g}_{\boldsymbol{m}} \boldsymbol{\mu}_g + \hat{e}^\dagger_{\boldsymbol{n}} \hat{e}_{\boldsymbol{m}} \boldsymbol{\mu}_e) \cdot \langle \boldsymbol{n}|\boldsymbol{B}(\boldsymbol{R})|\boldsymbol{m}\rangle, \end{aligned} \tag{10}$$

where $\hat{\Sigma}_{\boldsymbol{n},\boldsymbol{m}} = \hat{g}^\dagger_{\boldsymbol{n}} \hat{e}_{\boldsymbol{m}}$ are ladder operators destroying an excited atom in trap state $\boldsymbol{m}$ and creating a ground-state atom in trap state $\boldsymbol{n}$. The semiclassical drive is now written as

$$\mathcal{H}_{\rm drive} = \Omega \sum_{\boldsymbol{n},\boldsymbol{m}} \hat{\Sigma}_{\boldsymbol{n},\boldsymbol{m}} \eta_{\boldsymbol{n},\boldsymbol{m}} + \hat{\Sigma}^\dagger_{\boldsymbol{n},\boldsymbol{m}} \eta_{\boldsymbol{n},\boldsymbol{m}}, \tag{11}$$

where we define the Franck-Condon factors $\eta_{\boldsymbol{n},\boldsymbol{m}} = \langle \boldsymbol{n}|e^{-\mathrm{i}\boldsymbol{k}_\ell \boldsymbol{R}}|\boldsymbol{m}\rangle = \int d\boldsymbol{R} [\phi_{\boldsymbol{n}}(\boldsymbol{R})]^* e^{-\mathrm{i}\boldsymbol{k}_\ell \boldsymbol{R}} \phi_{\boldsymbol{m}}(\boldsymbol{R})$. For tight trapping conditions, where the localization of the atoms is on a level much smaller than the wavelength $2\pi/k_\ell$, the exponential can be approximated with unity and the Franck-Condon factors are equal to $\delta_{\boldsymbol{nm}}$. In addition, to take into account the first-order correction, a Lamb-Dicke limit approximation can be made and only the matrix elements of the linear term $\mathrm{i}\boldsymbol{k}_\ell \boldsymbol{R}$ would need to be considered.

III. QUANTUM NONDEGENERATE GAS LIMIT

Let us now focus on the semiclassical case, which assumes classical dynamics for the atomic motion, while the electronic dynamics is described in a quantum fashion in terms of Pauli matrices. As a function of the drive intensity, the emergent physics can be quite distinct. In a first case, where a high-intensity drive is assumed, high-excitation levels can be reached, with many atoms being excited at the same time. This is the standard regime for Dicke superradiance, i.e., the quick burst of spontaneous emission from an initial fully excited ensemble of closely spaced atoms. The other limit we consider is the weak-excitation limit, where there are hardly any excitations present in the system, rendering it possible to perform a transformation to a fully classical coupled dipole model. Despite its simplicity, the weak-excitation limit gives insights into the emergence of cooperative effects and their role in modifying the directional scattering of light. In particular, we emphasize the role of magnetic dipole-dipole interactions and their competition with the widely studied electric counterpart.

A. Effective spin Hamiltonian

From the Hamiltonian listed in Eq. (3), one can derive a master equation for the evolution of the $\mathcal{N}$ electronic systems under the approximation of a frozen gas. Such an approximation can hold for low-enough temperatures, where motion evolution is slow compared to the time taken by any radiative processes. The derivation is based on the elimination of the photonic degrees of freedom [22–24,34,35], as outlined in detail in Appendixes B, C, D, and E. The effective Hamiltonian describing dynamics in the reduced subspace of dimension $2^{\mathcal{N}}$ of the electronic degrees of freedom reads

$$\begin{aligned}\mathcal{H}_{\rm eff} = &\Delta \sum_i \sigma_i^\dagger \sigma_i + \sum_{i\neq j} \big(g^{(d)}_{ji} + g^{(\mu)}_{ji}\big) \sigma_i^\dagger \sigma_j \\ &+ \Omega \sum_i (e^{-\mathrm{i}\boldsymbol{R}_i \boldsymbol{k}_\ell} \sigma_i + e^{\mathrm{i}\boldsymbol{R}_i \boldsymbol{k}_\ell} \sigma_i^\dagger) \\ &+ \frac{1}{8} \sum_{i\neq j} \Omega^{e,e}_{i,j} \big(1+\sigma_i^z\big)\big(1+\sigma_j^z\big) \\ &+ \frac{1}{8} \sum_{i\neq j} \Omega^{g,g}_{i,j} \big(1-\sigma_i^z\big)\big(1-\sigma_j^z\big) \\ &+ \frac{1}{4} \sum_{i\neq j} \Omega^{g,e}_{i,j} \big(1-\sigma_i^z\big)\big(1+\sigma_j^z\big). \end{aligned} \tag{12}$$

This describes the unitary part of the interaction corresponding to a full-fledged spin-1/2 XXZ model. Here the detuning is defined as $\Delta = \omega - \omega_\ell$. The second term gives the usual electric and magnetic dipole-dipole interactions allowing for the hopping of excitations within the whole ensemble, describing the XY part. The last three terms represent the contribution from the static magnetic interactions and lead to frequency shifts conditioned on the occupancy of the pair of atoms involved in the interaction, which is typically referred to as an effective Ising interaction. The coherent photon exchange via electric dipole-dipole interactions $g^{(d)}_{ji}$ has been widely studied [19]. The magnetic transition dipole-dipole couplings $g^{(\mu)}_{ji}$ generally can be ignored as they are of very small magnitude compared to the electric ones. However, other important couplings occur

$$\Omega^{\alpha,\beta}_{i,j} = \frac{\mu_0}{4\pi R^3_{ij}} \left[3 \frac{(\boldsymbol{\mu}_{i,\alpha}\cdot\boldsymbol{R}_{ij})(\boldsymbol{\mu}_{j,\beta}\cdot\boldsymbol{R}_{ij})}{R^2_{ij}} - \boldsymbol{\mu}_{i,\alpha}\cdot\boldsymbol{\mu}_{j,\beta} \right], \tag{13}$$

with $\alpha, \beta \in \{e, g\}$, which describe magnetic dipole interactions between atoms owing to the static magnetic dipoles, illustrated in Fig. 2 on the right side. This is an interaction between the electronic ground and excited state densities as opposed to a spin-flip interaction for transition dipoles.

With the elimination of the electromagnetic vacuum, the system is characterized by open system dynamics where the collective dissipation is included in the master equation

$$\frac{d\rho}{dt} = -\mathrm{i}[\mathcal{H}_{\rm eff}, \rho] + \mathcal{L}_\mu[\rho] + \mathcal{L}_d[\rho]. \tag{14}$$

We assume standard Lindblad form for the loss terms which we write as follows:

$$\mathcal{L}_\alpha[\rho] = \sum_{i,j=1}^{\mathcal{N}} f^{(\alpha)}_{ij} (2\sigma_i \rho \sigma_j^\dagger - \{\sigma_j^\dagger \sigma_i, \rho\}). \tag{15}$$

The independent radiative loss rates are $\Gamma = k_0^3 d^2/(3\pi\hbar\epsilon_0)$ and $\Gamma_\mu = k_0^3 \mu^2/3\pi\hbar\epsilon_0$ stemming from electric and magnetic

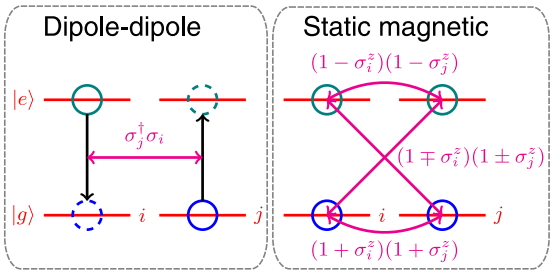

FIG. 2. Illustration of interactions present in the effective Hamiltonian Eq. (12). On the left is the excitation hopping due to the electronic dipole interaction between sites i and j. Initial occupations are indicated in filled open circles and the final occupations in dotted open circles. As indicated by the filled circle, the initially excited state on site i is changed to the ground state by σ_i. Similarly, the ground state on site j, indicated by a filled circle is excited due to $\sigma_j^\dagger$. On the right side is the density-density interaction due to the static magnetic dipole interaction with the same color coding. Here, either the ground or excited state can be occupied on i and j, leading to different interactions indicated by arrows between them and annotated with the appropriate interaction terms.

contributions. Moreover, collective dissipation at rates $f_{ij}^{(d)}$ (electric) and $f_{ij}^{(\mu)}$ (magnetic) are also present, with the exact expressions listed in Appendix E. The magnitude of Γ depends on the particular transition we consider, but it is around $\Gamma \approx 1$ MHz so that $f_{ij}^{(d)} \approx 1$ MHz particles at distance λ. We usually also choose Δ to be of the order of Γ, while $f_{ij}^{(\mu)}$ is negligible.

B. Weak-excitation limit: Coupled dipoles model

The Hamiltonian in Eq. (12) is of general validity in the quantum nondegenerate regime. However, by considering the weak-excitation limit, the evolution of the system is restricted to a very small subspace where the analytical description of the dynamics can be greatly simplified. In addition, we set the magnetic transition dipole moment to zero so that $f_{ij}^{(\alpha)} = g_{ij}^{(\alpha)} = 0$ since it is negligible. To do this, we linearize the time evolution of the system by replacing all population operators with -1 and factorizing all two operator correlations. We gather all expectation values of atomic coherences in a single vector $\boldsymbol{v} = (\langle\sigma_1\rangle, \ldots, \langle\sigma_{\mathcal{N}}\rangle)^\top$ and write an effective first-order differential equation

$$\dot{\boldsymbol{v}}(t) = -i\mathcal{M}\boldsymbol{v}(t) + \Omega\boldsymbol{v}_{\text{drive}}, \tag{16}$$

which is derived in Appendices E and F where the drive vector incorporates all the drive phases $\boldsymbol{v}_{\text{drive}} = (e^{i\boldsymbol{k}_\ell\boldsymbol{R}_1}, \ldots, e^{i\boldsymbol{k}_\ell\boldsymbol{R}_{\mathcal{N}}})^\top$. The weak driving approximation $\Omega \ll |\boldsymbol{f}^{(d)}|$ assumes that the Rabi frequency is much weaker than the dissipative part of the dipole-dipole interaction. Notice also that the equation above can be solved both in the steady state to derive spectroscopic features of the ensemble as well as in the time domain (by imposing a time dependence on Ω). The matrix $\mathcal{M}$ incorporates both coherent and dissipative cooperative behavior

$$\mathcal{M}_{jj'} = [\Delta + \delta\omega_j]\delta_{jj'} - \left[g_{jj'}^{(d)} + \mathrm{i}f_{jj'}^{(d)}\right]. \tag{17}$$

We use the low-excitation condition in order to approximate $\langle\sigma_j^z\sigma_{j'}\rangle \approx -\langle\sigma_{j'}\rangle$. This is always true if $j = j'$, but only approximately valid under the condition that very few excitations are present in the system such that, on average, each site has a much lower than unit population in the excited state. This leads to the definition of a local frequency shift

$$\begin{aligned}\delta\omega_j &= \sum_{j'\neq j}\left(\Omega_{jj'}^{e,g} - \Omega_{jj'}^{g,g}\right)\\ &= \frac{(\mu_e-\mu_g)\mu_g\mu_0}{4\pi}\sum_{j'\neq j}\frac{3z_{jj'}^2/R_{jj'}^2 - 1}{R_{jj'}^3},\end{aligned} \tag{18}$$

where $\delta\omega_j$ denotes the total shift acquired owing to magnetic interactions. Since the particle positions are drawn from random configurations due to the thermal motion, this amounts to an effect of frequency disorder. We assume that all magnetic dipole moments in the ground state are $\mu_g \parallel \hat{e}_z$ and all magnetic moments in the excited state are $\mu_e \parallel \hat{e}_z$. We also take the electric dipole moments to be the same and belonging to a transition that emits circularly polarized light $\boldsymbol{d}_i \parallel (1, \pm\mathrm{i}, 0)^T$ (the sign does not matter due to the symmetry of the cloud) and a laser with the same polarization. This leads to the definition of the magnetic interaction rate

$$\Omega_\mu = \frac{\mu_0(\mu_e-\mu_g)\mu_g}{4\pi}. \tag{19}$$

For $\mu_g = 10$ an estimate of the effect of the magnetic interactions leads to $\Omega_\mu = 0.\,815\ \text{MHz} \times \text{nm}^3$. Additionally, we neglect contributions from the magnetic transition dipole moments' couplings as they are much smaller than the electrically mediated couplings and we neglect the magnetic field induced by the electric dipole moments. We then consider the coherent part of the far-field intensity radiated by a system defined by these dipoles in the xy plane

$$I(\boldsymbol{r}_s) \propto \left|\sum_i e^{-i\boldsymbol{k}_s\boldsymbol{R}_i}v_i\right|^2, \tag{20}$$

where $\boldsymbol{r}_s$ indicates the detection angle, $\boldsymbol{k}_s \parallel \boldsymbol{r}_s$ and $|\boldsymbol{k}_s| = k_0$ is the wave vector for the propagation in the detection direction.

In the steady state, assuming time-independent driving, the linear system obtained from setting the left-hand side of Eq. (16) to zero has to be solved. In practice, this equation needs to be solved for many different configurations. Since we assume the cloud to be thermal, we assume this particle distribution with respect to the center of the cloud to be Gaussian. When the atomic motion timescale is much slower than $1/\Gamma$, i.e., the Doppler shift ω_d is much smaller than Γ, averaging over these different configurations corresponds to a thermal average. The velocities do not contribute since the Doppler shift is negligible and a detector will average over the different configurations the cloud assumes.

In Fig. 3(a), we can see that static magnetic dipolar interaction reduces the forward enhancement due to constructive interference of the emitted light in the laser direction. The inhomogeneous broadening reduces this constructive interference so that the forward enhancement is reduced as well. Alternatively, this can be reinterpreted when we consider that the frequency disorder generates matrix elements between different phase configurations in the atomic ensemble so that

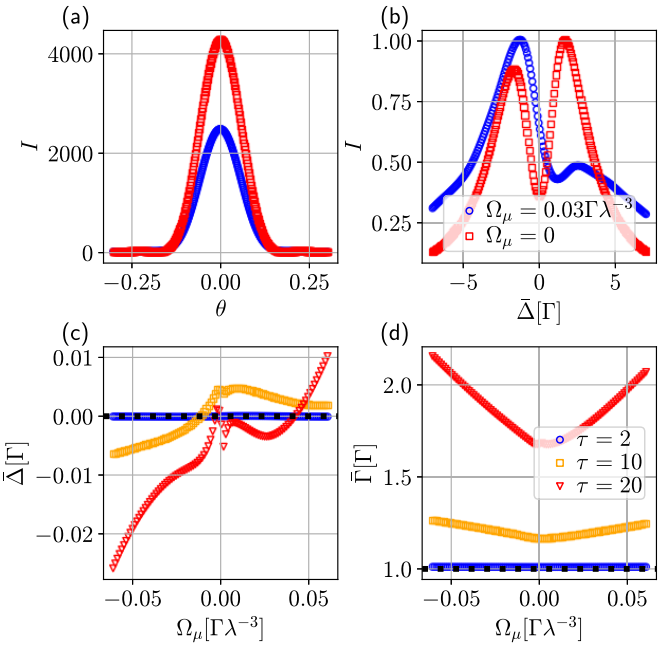

FIG. 3. Numerical results based on solution of Eq. (16) in the steady state. We consider multiple configurations of a cloud where the particles are distributed according to a Gaussian probability distribution with optical depth $\tau = 3\mathcal{N}/(2k_0^2R^2)$, simulating averaging over atomic motion. The number of configurations is $\mathcal{N}_c = 1000$ and $\mathcal{N} = 1000$. The optical depth is $\tau = 15$. Ω_μ quantifies the strength of the magnetic interaction. In (a) we show how the forward enhancement is modified by the magnetic interaction by plotting the intensity variation versus the in-plane angle θ on the single-particle resonance $\Delta = 0$. There is a reduction in the forward enhancement for $\Omega_\mu = 0.03\Gamma\lambda^3$ compared to no magnetic interaction. In (b) we investigate the lineshape of the cloud by changing the laser detuning Δ and compare $\Omega_\mu = 0.03\Gamma\lambda^3$ with $\Omega_\mu = 0$ at an in-plane detection angle of $\theta = \pi/10$. The double peak structure in the nonmagnetic case becomes asymmetric when the magnetic interaction is turned on. Changing the sign flips the effect on the two peaks (not shown). In (c) and (d) we investigate the effect of the magnetic interaction on the cooperative properties of the sample. To this end we determine the collective lineshift $\bar{\Delta}$ and the collective linewidth $\bar{\Gamma}$ in the forward direction $\theta = 0$ by calculating the lineshapes and then extracting these parameters from a Lorentzian fit. The lineshift and linewidth enhancement are shown for different optical densities τ with the magnetic interaction strength on the x-axis.

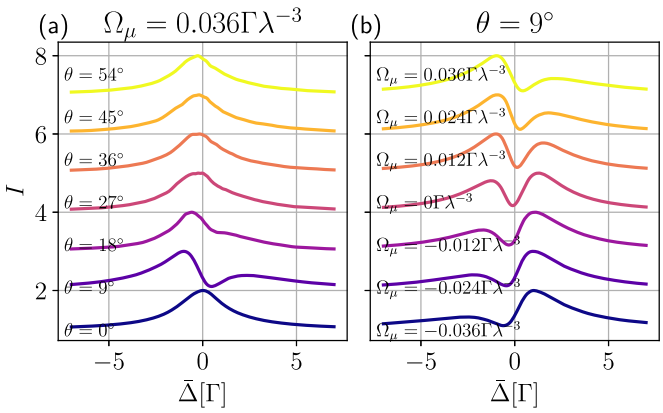

FIG. 4. Numerical results based on the solution of Eq. (16) in the steady state. We show for $N = 1000$ particles and averaging over $N_c = 1000$ runs the normalized lineshapes for different transversal angles θ in (a) and different magnetic interaction strengths Ω_μ in (b). The calculations are performed for a spherical Gaussian cloud with optical density $\tau = 25$.

more light is scattered into angles other than the laser-driven direction. Furthermore, we observe a double peak structure of the lineshape at a shallow detection angle of $\pi/10$ in Fig. 3(b), which was previously attributed to vacuum Rabi splitting in Ref. [36] and also observed in Ref. [18]. We discuss this in more detail when interpreting Fig. 4. In Figs. 3(c) and 3(d) we perform studies of the lineshift and linewidth modification due to the presence of the magnetic interaction for different optical densities τ. From the lineshift we can estimate the total symmetric contribution to the frequency shift of the ensemble, which causes a lineshift that depends on the sign of the magnetic dipole-dipole interaction. From the linewidth enhancement one can see the effect of the asymmetric contribution to the frequency disorder, i.e., the inhomogeneous broadening. From the results for $\tau = 20$ it is fairly clear that there are two different regimes. For large magnetic interaction Ω_μ the large frequency disorder simply leads to an inhomogeneous linewidth enhancement. For smaller $\Omega_\mu \approx 0.005\lambda^3\Gamma$ the linewidth is decreased. One explanation for this is that frequency disorder facilitates scattering into states that are naturally more subradiant than the originally driven state without disorder. Furthermore, we make connections between the quantities plotted here and the scaling of the features observed with the particle number N, the optical density τ, and the peak density n_0 of the cloud. First, consider Ref. [36] where it is shown that the optical density is the relevant parameter when investigating effects due to the electric dipole transition such as the observed double peak structure. Keeping the optical density τ constant, the peak density will then scale with the particle number $n_0 \propto \sqrt{N}\tau$ so that the density can be tuned via particle number at constant optical density. We then identify that the magnitude of the static magnetic dipolar interaction depends on the density of the cloud so that the magnetic interaction strength Ω_μ acts as a proxy for both density and particle number.

IV. CONCLUSION

We described the emission and scattering properties of a dense atomic cloud for distinguishable, classically moving particles. We made use of an open quantum system approach where we showed that tunable spin Hamiltonians can be designed. In addition, under the assumption of weak external drive, and in particular, for atoms where magnetic interactions are strong, we characterized their effects on the properties of scattered light. For quantum degenerate gases, we introduced the relevant Hamiltonian including electric and magnetic dipole interactions and provided a quick outlook of how one would proceed in analyzing their emission properties in an externally dictated trap basis. In the future, we will augment this approach to the full open system formulation to derive the interplay between quantum statistics and quantum

electromagnetic vacuum effects such as super and subradiance. We expect that our findings are of relevance for dense atomic dysprosium clouds for which a short description of a possible experimental implementation is presented in Appendix A. The setup is, in principle, fairly standard consisting of a cooling setup where Dysprosium atoms are Zeeman-slowed and then trapped and laser-cooled in a magnetooptical trap (MOT). This allows the tuning of the cloud density and particle number and hence the parameters varied in our simulations. If the sample is sufficiently cold, the quantum degenerate regime can also be reached in this setup so that both the quantum nondegenerate and degenerate regimes can be investigated.

ACKNOWLEDGMENTS

We acknowledge financial support from the Max Planck Society and from the Deutsche Forschungsgemeinschaft (DFG, German Research Foundation) Project-ID 429529648–TRR 306 QuCoLiMa ("Quantum Cooperativity of Light and Matter").

APPENDIX A: POSSIBLE EXPERIMENTAL REALIZATION

To experimentally observe the effects discussed in the main body of the article, we developed and built an apparatus to cool and trap neutral dysprosium [37]. Dysprosium belongs to the group of lanthanide elements whose characteristic open f-shell electron configuration $[\mathrm{Xe}]4f^{10}6s^2$ with spin $S = 2$, orbital angular momentum $L = 6$, and total angular momentum $J = 8$ gives rise to its high magnetic moment of 10 Bohr magnetons ($\mu_g \sim 10\mu_B$). Compared to alkali atoms whose magnetic moments are on the order of only $\mu_g \sim 1\mu_B$, the magnetic dipole-dipole interactions in ultracold gases of dysprosium is about 100 times stronger, making it an ideal candidate for investigating its contribution to cooperative effects. In addition, there is an almost equal abundance of stable bosonic and fermionic isotopes allowing for the creation of both types of quantum degenerate gases [38,39].

The general experimental scheme for producing laser cooled samples of lanthanide atoms is implemented as follows [40,41]: A strong optical transition in the blue spectrum range is used to precool the atoms in a Zeeman slower (ZS) before capturing them in a narrow line magnetooptical trap (MOT). Operating a MOT on transitions with natural linewidths on the order of 100 kHz is required to reach Doppler temperatures 5 μK, which allows one to directly transfer the atoms from the MOT into an optical dipole trap (ODT). In our setup, we employ a strong $J = 8 \rightarrow J' = 9$ transition at 421 nm, with a natural linewidth of $\Gamma_{421} = 2\pi \cdot 32$ MHz for precooling. A thermal beam of atomic dysprosium, transversally cooled on this broad transition, reaches the ZS with initial velocities of several hundred meters per second. The atoms are then longitudinally decelerated to a velocity of about 24 m/s in the spin-flip configuration ZS before entering the main chamber, where they are captured in a six beam three-dimensional (3D) MOT setup. The MOT transition, on the other hand, is a closed, narrow linewidth $J = 8 \rightarrow J' = 9$ transition at 626 nm with a natural linewidth of $\Gamma_{626} = 2\pi \times 136$ kHz which corresponds to a Doppler temperature of 3.2 μK.

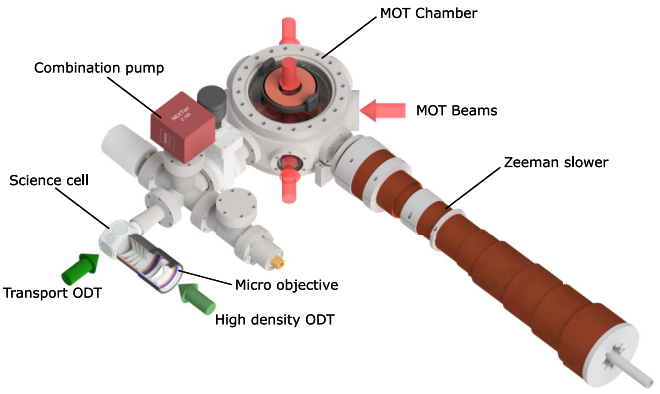

FIG. 5. CAD render of the vacuum system. Dysprosium atoms reach the ZS with a velocity of few hundred meters per second. They are longitudinally slowed in the ZS with resonant laser light at the 421 nm before being captured in a narrow line 3D MOT at 626 nm. An achromatic lens in conjunction with an air-bearing translation stage is used to focus down the optical transport beam at the position of the MOT and create a deep ODT. The focal spot of this beam is then moved from the MOT chamber to the center of the science cell by moving the translation stage, thereby transferring the atoms alongside. To retain a substantial number of atoms in the trap after this sequence, the process of transport and retrapping of atoms needs to be done on a timescale that is shorter than the lifetime of the ODT.

Our experimental setup consists of a high numerical aperture (NA) science cell connected to an ultrahigh vacuum (UHV) chamber (MOT) and a dedicated laser system capable of generating tunable and frequency stabilized laser radiation. Consequently, the laser frequency can be readily adapted to capture either bosons or fermions without any optical or mechanical adjustments. Figure 5 shows a CAD render of the vacuum system. To reduce the influence of undesired external magnetic fields, the vacuum system is assembled exclusively from nonmagnetic stainless steel, titanium, and ceramic glass. Additionally, a commercial, three-axis magnetic-field compensation system (Stefan Mayer Instruments GmbH: MR-3) is used to drive a 3D coil system and compensate low frequency magnetic-field disturbances.

The next step for creating dense samples of atomic dysprosium is to transfer atoms to the science cell attached to the MOT chamber. The cell offers a high optical access (with nine optical view ports), is designed in-house, and made out of the machinable glass-ceramic MACOR (Corning Inc.). A deep ODT at the MOT position will be created, using a diode pumped solid-state (DPSS) laser (Coherent: Mephisto MOPA 55 W) to transport the atoms. This will be achieved by using an achromatic lens to focus down the transport beam to a beam waist of $w_0 \sim 66$ μm and two mirrors mounted on an air-bearing translation stage (Aerotech: ABL1500-300), which enables reproducible and precise movement of the focal spot of the beam, thereby, transporting the atoms alongside [42]. The atoms are retrapped inside the science cell using a custom made multilens micro-objective, designed to offer diffraction-limited performance at the trapping wavelength of 1064 nm [43,44]. A five-lens configuration consisting solely of commercial singlets was chosen to achieve a high NA of 0.53 and a working distance of 22 mm. Simulation and

optimization of objective parameters like lens curvature, relative spacing, and thickness was done using a ray-tracing software (OPTICSTUDIO) to minimize optical aberrations and achieve diffraction-limited performance. The beam waist at the focus of the micro-objective was measured using a piezo-controlled knife edge and found to be $w_{0h} = 5.94 \pm 1.18$ µm and $w_{0v} = 6.99 \pm 0.67$ µm, in the horizontal and vertical directions, respectively. We estimate that an ODT created with this objective should provide a sufficiently tight confinement for a few hundred to a few thousand dysprosium atoms to reach densities on the order of $\sim 10^{13}$ atoms/cm^3. This condition would then allow us to explore dynamics in the high-density regime where the interparticle/interemitter spacing is lower than the wavelength of the exciting transition, giving rise to effects like Dicke sub and superradiance.

APPENDIX B: MAGNETIC INTERACTION TERMS IN LIGHT MATTER HAMILTONIAN FROM FIRST PRINCIPLES

We will be using the following definitions for the gauge field, electric, and magnetic field operators

$$\hat{\boldsymbol{A}} = \sum_{\boldsymbol{k},\boldsymbol{\epsilon}} g_k \boldsymbol{\epsilon_k} (\hat{a}_{\boldsymbol{k},\boldsymbol{\epsilon}} e^{\mathrm{i}\boldsymbol{kR}} + \hat{a}^\dagger_{\boldsymbol{k},\boldsymbol{\epsilon}} e^{-\mathrm{i}\boldsymbol{kR}}), \tag{B1}$$

$$\hat{\boldsymbol{E}} = \mathrm{i} \sum_{\boldsymbol{k},\boldsymbol{\epsilon}} g_k \omega_k \boldsymbol{\epsilon_k} (\hat{a}_{\boldsymbol{k},\boldsymbol{\epsilon}} e^{\mathrm{i}\boldsymbol{kR}} - \hat{a}^\dagger_{\boldsymbol{k},\boldsymbol{\epsilon}} e^{-\mathrm{i}\boldsymbol{kR}}), \tag{B2}$$

$$\hat{\boldsymbol{B}} = \mathrm{i} \sum_{\boldsymbol{k},\boldsymbol{\epsilon}} (\boldsymbol{k} \times \boldsymbol{\epsilon_k}) g_k (\hat{a}_{\boldsymbol{k},\boldsymbol{\epsilon}} e^{\mathrm{i}\boldsymbol{kR}} - \hat{a}^\dagger_{\boldsymbol{k},\boldsymbol{\epsilon}} e^{-\mathrm{i}\boldsymbol{kR}}), \tag{B3}$$

with $g_k = 1/\sqrt{2\omega_k \mathcal{V} \epsilon_0}$ photon coupling strength with photonic operators as defined in the main text.

If we omit terms where the square of the gauge field appears and the term where the atom core momentum is coupled to the gauge field (amounting to a Born-Oppenheimer and subsequently a rotating wave approximation), the simplified Hamiltonian is composed of three parts, written in the Coulomb gauge

$$\mathcal{H} \approx \mathcal{H}_0 + \mathcal{H}_{\mathrm{af}} + \mathcal{H}_{\mathrm{dipole}}, \tag{B4}$$

$$\mathcal{H}_0 = \sum_i^N \frac{\hat{\boldsymbol{P}}_i^2}{2M} + \frac{\hat{\boldsymbol{p}}_i^2}{2m} + V_{ec}(\boldsymbol{R}_i, \boldsymbol{r}_i), \tag{B5}$$

$$\mathcal{H}_{af} = \frac{1}{m} \sum_i^N \hat{\boldsymbol{A}}(\boldsymbol{r}_i) \cdot \hat{\boldsymbol{p}}_i, \tag{B6}$$

$$\mathcal{H}_{\mathrm{dipole}} = \frac{1}{2} \sum_{i \neq j} \sum \frac{\boldsymbol{d}_i \cdot \boldsymbol{d}_j - 3(\boldsymbol{R}_{ij}\boldsymbol{d}_i)(\boldsymbol{R}_{ij} \cdot \boldsymbol{d}_j)}{R_{ij}^3}. \tag{B7}$$

where we already performed a dipole approximation for the Coulomb interaction between different atoms leading to the explicit form of $\mathcal{H}_{\mathrm{dipole}}$. The Hamiltonian $\mathcal{H}_{af}$ is the canonical coupling between the electronic degree of freedom and the transverse modes of the light-field. We have not completed the dipolar approximation in the gauge field which still contains the position of the electron $\boldsymbol{r}_i$, which is a quantum operator in this description. The Hamiltonian $\mathcal{H}_0$ contains the electron kinetic energy, the center-of-mass kinetic energy, and the interaction between the electron and the core. The electron kinetic energy and the core-electron potential give rise to the level structure of the atom. We consider a Born-Oppenheimer picture where $\boldsymbol{R}_i$ represents the center of mass position.

Instead of making the usual dipolar approximation for the gauge field, we consider one order higher in the Taylor approximation of the electron position around the center-of-mass position $e^{\mathrm{i}\boldsymbol{kr}_i} \approx e^{\mathrm{i}\boldsymbol{kR}_i}[1 + \mathrm{i}\boldsymbol{kx}_i]$ with the distance vector $\boldsymbol{x}_i = \boldsymbol{r}_i - \boldsymbol{R}_i$. The atom field Hamiltonian then splits into two contributions

$$\begin{aligned}\mathcal{H}_{af} = &\frac{1}{m} \sum_i^N \hat{\boldsymbol{p}}_i \cdot \hat{\boldsymbol{A}}(\boldsymbol{R}_i) \\ &+ \mathrm{i} \sum_{\boldsymbol{k},\boldsymbol{\epsilon}} g_k (\hat{\boldsymbol{p}}_i \cdot \boldsymbol{\epsilon_k})(\boldsymbol{kx}_i)(\hat{a}_{\boldsymbol{k},\boldsymbol{\epsilon}} e^{\mathrm{i}\boldsymbol{kR}_i} - \hat{a}^\dagger_{\boldsymbol{k},\boldsymbol{\epsilon}} e^{-\mathrm{i}\boldsymbol{kR}_i}).\end{aligned} \tag{B8}$$

The first term is the simple dipole approximation which leads to the coupled dipole model after some additional approximations and a gauge transformation. The second term is of higher order and contains the magnetic and quadrupole electric moment as we will see. To see that the double dot product indeed yields the magnetic and quadrupole term, it needs to be rearranged

$$\begin{aligned}(\hat{\boldsymbol{p}}_i \cdot \boldsymbol{\epsilon_k})(\boldsymbol{k} \cdot \boldsymbol{x}_i) &= (\hat{\boldsymbol{p}}_i \cdot \boldsymbol{k})(\boldsymbol{x}_i \cdot \boldsymbol{\epsilon_k}) + (\boldsymbol{x}_i \times \hat{\boldsymbol{p}}_i)(\boldsymbol{k} \times \boldsymbol{\epsilon_k}) \\ &= \tfrac{1}{2}((\hat{\boldsymbol{p}}_i \cdot \boldsymbol{\epsilon_k})(\boldsymbol{k} \cdot \boldsymbol{x}_i) + (\hat{\boldsymbol{p}}_i \cdot \boldsymbol{k})(\boldsymbol{x}_i \cdot \boldsymbol{\epsilon_k})) \\ &\quad + \tfrac{1}{2}\hat{\boldsymbol{L}}(\boldsymbol{k} \times \epsilon_k).\end{aligned} \tag{B9}$$

The first term is the electronic quadrupole term whereas the second term contains the angular momentum implying that it is indeed the magnetic coupling. Summarizing the calculations above, the terms that must be added to the Hamiltonian if the dipole approximation is performed to higher order are

$$\begin{aligned}\mathcal{H}_m &= \mathrm{i} \sum_i^N \frac{\hat{\boldsymbol{L}}_i}{2m} \cdot \sum_{\boldsymbol{k},\boldsymbol{\epsilon}} g_k (\boldsymbol{k} \times \boldsymbol{\epsilon_k})(\hat{a}_{\boldsymbol{k},\boldsymbol{\epsilon}} e^{\mathrm{i}\boldsymbol{kR}_i} - \hat{a}^\dagger_{\boldsymbol{k},\boldsymbol{\epsilon}} e^{-\mathrm{i}\boldsymbol{kR}_i}) \\ &= \sum_i^N \hat{\boldsymbol{\mu}}_i \cdot \hat{\boldsymbol{B}}(\boldsymbol{R}_i), \\ \mathcal{H}_q &= \sum_{i,\boldsymbol{k},\boldsymbol{\epsilon}} \frac{\mathrm{i}|\boldsymbol{k}|}{2m} (p_{\boldsymbol{k}} r_{\boldsymbol{\epsilon}} + p_{\boldsymbol{\epsilon}} r_{\boldsymbol{k}}) g_k (\hat{a}_{\boldsymbol{k},\boldsymbol{\epsilon}} e^{\mathrm{i}\boldsymbol{kR}_i} - \hat{a}^\dagger_{\boldsymbol{k},\boldsymbol{\epsilon}} e^{-\mathrm{i}\boldsymbol{kR}_i}).\end{aligned} \tag{B10}$$

Here we avoid complications with spin degrees of freedom by making the association $\hat{\boldsymbol{\mu}}_i = -\frac{\hat{\boldsymbol{L}}_i}{2m}$ and noting that spin degrees of freedom need to be explicitly inserted into the Hamiltonian which ultimately change the definition of $\hat{\boldsymbol{\mu}}_i$. Since we go into a two-level picture this is, however, already taken care of and we need not consider these complications in detail.

APPENDIX C: REPRESENTATION OF THE HAMILTONIAN IN THE TWO-LEVEL APPROXIMATION

We perform a two-level approximation in which we assume there exist two relevant levels per atom, the ground state $|g_i\rangle$ and the excited state $|e_i\rangle$ separated by a frequency ω_0. Taking the projection of the momentum and magnetic moment operator onto this subspace, we can explicitly write the Hamiltonian using the matrix elements within this subspace. One relevant

point here is that the momentum operator has no diagonal components whereas the magnetic moment operator has no such symmetry restriction.

Omitting the quadrupole term, the atom-field Hamiltonian then becomes

$$\mathcal{H}_{\rm af} = \mathrm{i}\sum_i^N (\boldsymbol{d}_i\sigma_i - \boldsymbol{d}_i^*\sigma_i^\dagger)\cdot\hat{\boldsymbol{A}}(\boldsymbol{R}_i) + (\boldsymbol{\mu}_i\sigma_i + \boldsymbol{\mu}_i^*\sigma_i^\dagger + \boldsymbol{\mu}_{i,e}\sigma^\dagger\sigma + \boldsymbol{\mu}_{i,g}\sigma\sigma^\dagger)\cdot\hat{\boldsymbol{B}}(\boldsymbol{R}_i), \tag{C1}$$

with $\boldsymbol{d}_i = \langle g_i|\hat{x}_i|e_i\rangle$ and $\boldsymbol{\mu}_{i,e} = \langle g_i|\hat{\boldsymbol{\mu}}_i|e_i\rangle$ for the transition dipoles and $\boldsymbol{\mu}_{i,e} = \langle e_i|\hat{\boldsymbol{\mu}}_i|e_i\rangle$, $\boldsymbol{\mu}_{i,g} = \langle g_i|\hat{\boldsymbol{\mu}}_i|g_i\rangle$ for the static magnetic dipole moment. The sigma matrices are transition operators of the type $\sigma_i = |g_i\rangle\langle e_i|$.

APPENDIX D: UNITARY TRANSFORMATION INTO DIPOLAR GAUGE

The next step in deriving the light-matter Hamiltonian is the gauge transformation

$$U = \exp\left(-\mathrm{i}\sum_i^N \int_{\boldsymbol{r}_i}^{\boldsymbol{R}_i} d\boldsymbol{r}\cdot\hat{\boldsymbol{A}}(\boldsymbol{r})\right). \tag{D1}$$

We note here that the gauge-field operator commutes with the magnetic-field operator $[\hat{\boldsymbol{A}}(\boldsymbol{r}), \hat{\boldsymbol{B}}(\boldsymbol{r}')] = 0$ so that H_m is not affected by this transformation. The effect on the dipole electronic transition and the static dipole $\mathcal{H}_{\rm dipole}$ is as usual so that, after also performing a rotating wave approximation, the Hamiltonian is

$$\mathcal{H} = \omega\sum_i \sigma_i^\dagger\sigma_i + \sum_{\boldsymbol{k},\boldsymbol{\epsilon}} \omega_k \hat{a}_{\boldsymbol{k},\boldsymbol{\epsilon}}^\dagger \hat{a}_{\boldsymbol{k},\boldsymbol{\epsilon}} + \sum_i \hat{\boldsymbol{d}}_i\cdot\hat{\boldsymbol{E}}(\boldsymbol{R}_i) + (\hat{\boldsymbol{\mu}}_{t,i} + \hat{\boldsymbol{\mu}}_{s,i})\cdot\hat{\boldsymbol{B}}(\boldsymbol{R}_i), \tag{D2}$$

with definitions $\hat{\boldsymbol{d}}_j = \boldsymbol{d}\sigma_j + \boldsymbol{d}^*\sigma_j^\dagger$, $\hat{\boldsymbol{\mu}}_{t,i} = \boldsymbol{\mu}_i\sigma_i + \boldsymbol{\mu}_i^*\sigma_i^\dagger$ and $\hat{\boldsymbol{\mu}}_{s,i} = \boldsymbol{\mu}_{i,e}\sigma^\dagger\sigma + \boldsymbol{\mu}_{i,g}\sigma\sigma^\dagger$.

APPENDIX E: ELIMINATION OF PHOTONIC DEGREES OF FREEDOM FROM HAMILTONIAN

The last step in determining the effective system dynamics is to perform an adiabatic elimination of the light modes for this Hamiltonian Eq. (D2). The first step is to determine the equation of motion for the photonic operators

$$\frac{d\hat{a}_{\boldsymbol{k},\boldsymbol{\epsilon}}}{dt} = -\mathrm{i}\omega_k\hat{a}_{\boldsymbol{k},\boldsymbol{\epsilon}} + \sum_i g_k\omega_k(\hat{\boldsymbol{d}}_i\cdot\boldsymbol{\epsilon}_{\boldsymbol{k}})e^{-\mathrm{i}\boldsymbol{k}\hat{\boldsymbol{R}}_i} + \sum_i g_k([\hat{\boldsymbol{\mu}}_{t,i} + \hat{\boldsymbol{\mu}}_{s,i}]\cdot[\boldsymbol{k}\times\boldsymbol{\epsilon}_{\boldsymbol{k}}])e^{-\mathrm{i}\boldsymbol{k}\hat{\boldsymbol{R}}_i}, \tag{E1}$$

which can then be integrated to yield

$$\hat{a}_{\boldsymbol{k},\boldsymbol{\epsilon}}(t) = \hat{a}_{\boldsymbol{k},\boldsymbol{\epsilon}}(0)e^{-\mathrm{i}\omega_k t} + \int_0^t ds e^{-\mathrm{i}\omega_k(t-s)} \times \sum_i g_k\omega_k(\hat{\boldsymbol{d}}_i(s)\cdot\boldsymbol{\epsilon}_{\boldsymbol{k}})e^{-\mathrm{i}\boldsymbol{k}\hat{\boldsymbol{R}}_i} + \int_0^t ds e^{-\mathrm{i}\omega_k(t-s)} \times \sum_i g_k([\hat{\boldsymbol{\mu}}_{t,i}(s) + \hat{\boldsymbol{\mu}}_{s,i}(s)]\cdot[\boldsymbol{k}\times\boldsymbol{\epsilon}_{\boldsymbol{k}}])e^{-\mathrm{i}\boldsymbol{k}\hat{\boldsymbol{R}}_i}. \tag{E2}$$

A simplification for the calculation that follows is to consider negative and positive frequency components of the magnetic and electric field, in particular,

$$\hat{\boldsymbol{B}}^\pm = \pm\mathrm{i}\sum_{\boldsymbol{k},\boldsymbol{\epsilon}} (\boldsymbol{k}\times\boldsymbol{\epsilon}_{\boldsymbol{k}})g_k\hat{a}_{\boldsymbol{k},\boldsymbol{\epsilon}}e^{\pm\mathrm{i}\boldsymbol{k}\boldsymbol{R}},$$
$$\hat{\boldsymbol{E}}^\pm = \pm\mathrm{i}\sum_{\boldsymbol{k},\boldsymbol{\epsilon}} g_k\omega_k\boldsymbol{\epsilon}_{\boldsymbol{k}}\hat{a}_{\boldsymbol{k},\boldsymbol{\epsilon}}e^{\pm\mathrm{i}\boldsymbol{k}\boldsymbol{R}}, \tag{E3}$$

so that we only have to consider the equation of motion for one of the photonic operators. To shorten the notation we also introduce the total magnetic dipole operator $\hat{\boldsymbol{\mu}}_i(t) = \hat{\boldsymbol{\mu}}_{t,i}(t) + \hat{\boldsymbol{\mu}}_{s,i}(t)$ leading to expressions for the positive field components of the electric and magnetic fields

$$\hat{\boldsymbol{E}}^+(\boldsymbol{R}_i) = \hat{\boldsymbol{E}}_0^+(\boldsymbol{R}_i) + \mathrm{i}\sum_{\boldsymbol{k},\boldsymbol{\epsilon},j}(g_k\omega_k)^2 e^{\mathrm{i}\boldsymbol{k}\boldsymbol{R}_{ij}}\boldsymbol{\epsilon}_{\boldsymbol{k}}\int_0^t ds e^{-\mathrm{i}\omega_k(t-s)}(\hat{\boldsymbol{d}}_j(s)\cdot\boldsymbol{\epsilon}_{\boldsymbol{k}}) + \mathrm{i}\sum_{\boldsymbol{k},\boldsymbol{\epsilon},j} g_k^2\omega_k e^{\mathrm{i}\boldsymbol{k}\boldsymbol{R}_{ij}}\boldsymbol{\epsilon}_{\boldsymbol{k}}\int_0^t ds e^{-\mathrm{i}\omega_k(t-s)}(\hat{\boldsymbol{\mu}}_i(s)\cdot[\boldsymbol{k}\times\boldsymbol{\epsilon}_{\boldsymbol{k}}]),$$
$$\hat{\boldsymbol{B}}^+(\boldsymbol{R}_i) = \hat{\boldsymbol{B}}_0^+(\boldsymbol{R}_i) + \mathrm{i}\sum_{\boldsymbol{k},\boldsymbol{\epsilon},j}(\boldsymbol{k}\times\boldsymbol{\epsilon}_{\boldsymbol{k}})g_k^2\omega_k e^{\mathrm{i}\boldsymbol{k}\boldsymbol{R}_{ij}}\int_0^t ds e^{-\mathrm{i}\omega_k(t-s)}(\hat{\boldsymbol{d}}_j(s)\cdot\boldsymbol{\epsilon}_{\boldsymbol{k}}) + \mathrm{i}\sum_{\boldsymbol{k},\boldsymbol{\epsilon},j}(\boldsymbol{k}\times\boldsymbol{\epsilon}_{\boldsymbol{k}})g_k^2 e^{\mathrm{i}\boldsymbol{k}\boldsymbol{R}_{ij}}\int_0^t ds e^{-\mathrm{i}\omega_k(t-s)}(\hat{\boldsymbol{\mu}}_i(s)\cdot[\boldsymbol{k}\times\boldsymbol{\epsilon}_{\boldsymbol{k}}]), \tag{E4}$$

where the zero subscript indicates that the photonic operators in the field expression were taken at time zero. Thus, both fields have similar terms. First, the vacuum time evolution, then the interaction with the proper dipole moment, and then a cross term between the magnetic and electric components of the interaction. There will be cross terms corresponding to the magnetic field produced by an electric dipole and the magnetic field produced by a magnetic dipole. Since we will neglect the magnetic transition dipole at the end of this treatment, we omit these cross terms and only keep the magnetic transition dipole terms to elucidate the difference to the magnetic static dipole term.

After the cross-terms are omitted, the total magnetic and electric field operators can be obtained from the positive frequency components by adding the hermitian conjugate so that after performing the usual summation over the polarization vectors

$$\hat{\boldsymbol{E}}(\boldsymbol{R}_i) = \hat{\boldsymbol{E}}_0(\boldsymbol{R}_i) + \mathrm{i}\sum_{\boldsymbol{k},j}(g_k\omega_k)^2 e^{\mathrm{i}\boldsymbol{k}\boldsymbol{R}_{ij}}\int_0^t ds e^{-\mathrm{i}\omega_k(t-s)}\cdot\left[\hat{\boldsymbol{d}}_j(s) - \frac{\boldsymbol{k}(\hat{\boldsymbol{d}}_j(s)\cdot\boldsymbol{k})}{k^2}\right] + \text{H.c.}, \tag{E5}$$

$$\hat{\boldsymbol{B}}(\boldsymbol{R}_i) = \hat{\boldsymbol{B}}_0(\boldsymbol{R}_i) + \mathrm{i}\sum_{\boldsymbol{k},j}(g_k\omega_k)^2 e^{\mathrm{i}\boldsymbol{k}\boldsymbol{R}_{ij}}\int_0^t ds e^{-\mathrm{i}\omega_k(t-s)}\cdot\left[\hat{\boldsymbol{\mu}}_i(s) - \frac{\boldsymbol{k}(\hat{\boldsymbol{\mu}}_i(s)\cdot\boldsymbol{k})}{k^2}\right] + \text{H.c.}, \tag{E6}$$

so that the magnetic and electric fields have the same structure. Now, the continuum limit is taken for the electromagnetic field modes $\frac{1}{V}\sum_{\boldsymbol{k}} \to \frac{1}{(2\pi)^3}\int d\boldsymbol{k}$ and the angular integral is performed in spherical coordinates so that, defining the dipolar Green's function

$$\begin{aligned}\mathbf{G}_k(\mathbf{R}) &= \left(\mathbb{1} + \frac{1}{k^2}\nabla\otimes\nabla\right)\frac{e^{\mathrm{i}kR}}{4\pi R}\\ &= \frac{e^{\mathrm{i}kR}}{4\pi k^2}\left[\left(\frac{k^2}{R} + \frac{\mathrm{i}k}{R^2} - \frac{1}{R^3}\right)\mathbb{1} + \left(-\frac{k^2}{R} - \frac{3\mathrm{i}k}{R^2} + \frac{3}{R^3}\right)\frac{\mathbf{R}\otimes\mathbf{R}}{R^2}\right],\end{aligned} \tag{E7}$$

with the usual shorthand $\boldsymbol{G}(\boldsymbol{R}) = \boldsymbol{G}_{k_0}(\boldsymbol{R})$ and the decomposition $\boldsymbol{G}_k(\boldsymbol{R}) = \boldsymbol{\Omega}_k(\boldsymbol{R}) - \mathrm{i}\boldsymbol{\Gamma}_k(\boldsymbol{R})$. The expressions for the electric and magnetic field become

$$\hat{\boldsymbol{E}}(\boldsymbol{R}_i) = \hat{\boldsymbol{E}}_0(\boldsymbol{R}_i) + \frac{\mathrm{i}}{\pi\epsilon_0}\sum_j\int_0^\infty dk\int_0^t ds k^2\boldsymbol{\Gamma}_{\boldsymbol{k}}(\boldsymbol{R}_{ij})\cdot\hat{\boldsymbol{d}}_j(s)e^{-\mathrm{i}\omega_k(t-s)} + \text{H.c.}, \tag{E8}$$

$$\hat{\boldsymbol{B}}(\boldsymbol{R}_i) = \hat{\boldsymbol{B}}_0(\boldsymbol{R}_i) + \frac{\mathrm{i}}{\pi\epsilon_0}\sum_j\int_0^\infty dk\int_0^t ds k^2\boldsymbol{\Gamma}_{\boldsymbol{k}}(\boldsymbol{R}_{ij})\cdot\hat{\boldsymbol{\mu}}_j(s)e^{-\mathrm{i}\omega_k(t-s)} + \text{H.c.}. \tag{E9}$$

The key is now that this elimination cannot be performed exactly and one must make a perturbative ansatz by plugging the time evolution of the dipole operators without light-matter interactions into these integrals. The free-space time evolution of the dipole operators is explicitly

$$\begin{aligned}\hat{\boldsymbol{d}}_j(s) &= \boldsymbol{d}\sigma_j(s) + \boldsymbol{d}^*\sigma_j^\dagger = \boldsymbol{d}\sigma_j(t)e^{-\mathrm{i}\omega(s-t)} + \boldsymbol{d}^*\sigma_j(t)^\dagger e^{\mathrm{i}\omega(s-t)},\\ \hat{\boldsymbol{\mu}}_{t,j}(s) &= \boldsymbol{\mu}_j\sigma_j(s) + \boldsymbol{\mu}_j^*\sigma_j^\dagger(s) = \boldsymbol{\mu}_j\sigma_j(t)e^{-\mathrm{i}\omega(s-t)} + \boldsymbol{\mu}_j^*\sigma_j^\dagger(t)e^{\mathrm{i}\omega(s-t)},\\ \hat{\boldsymbol{\mu}}_{s,j}(s) &= \boldsymbol{\mu}_{j,e}\sigma_j^\dagger(s)\sigma_j(s) + \boldsymbol{\mu}_{j,g}\sigma_j(s)\sigma_j^\dagger(s) = \hat{\boldsymbol{\mu}}_{s,j}(t).\end{aligned} \tag{E10}$$

This implies that the fundamental difference between the static and transition dipole moments is given by the frequency they rotate at. All these time evolutions will lead to integrations of the type

$$\zeta(\omega) = \mathrm{i}\int_0^\infty e^{\mathrm{i}\omega t}dt = \mathcal{P}\frac{1}{\omega} + \mathrm{i}\pi\delta(\omega), \tag{E11}$$

so that splitting the magnetic field into a transition part $\hat{\boldsymbol{B}} = \hat{\boldsymbol{B}}_t + \hat{\boldsymbol{B}}_s$ while keeping the vacuum contribution in the transition part

$$\begin{aligned}\hat{\boldsymbol{E}}(\boldsymbol{R}_i) &= \hat{\boldsymbol{E}}_0(\boldsymbol{R}_i) + \frac{1}{\pi\epsilon_0}\sum_j\int_0^\infty dk k^2\boldsymbol{\Gamma}_k(\boldsymbol{R}_{ij})\cdot\boldsymbol{d}(\sigma_j\zeta(\omega_k+\omega) + \sigma_j^\dagger\zeta(\omega_k-\omega)) + \text{H.c.},\\ \hat{\boldsymbol{B}}_t(\boldsymbol{R}_i) &= \hat{\boldsymbol{B}}_0(\boldsymbol{R}_i) + \frac{1}{\pi\epsilon_0}\sum_j\int_0^\infty dk k^2\boldsymbol{\Gamma}_k(\boldsymbol{R}_{ij})\cdot\boldsymbol{\mu}_{t,j}(\sigma_j\zeta(\omega_k+\omega) + \sigma_j^\dagger\zeta(\omega_k-\omega)) + \text{H.c.},\\ \hat{\boldsymbol{B}}_s(\boldsymbol{R}_i) &= \frac{1}{\pi\epsilon_0}\sum_j\int_0^\infty dk k^2\boldsymbol{\Gamma}_k(\boldsymbol{R}_{ij})\cdot\boldsymbol{\zeta}(\omega_k)(\boldsymbol{\mu}_{j,e}\sigma_j^\dagger\sigma_j + \boldsymbol{\mu}_{j,g}\sigma_j\sigma_j^\dagger) + \text{H.c.}.\end{aligned} \tag{E12}$$

The previous statement about the rotational frequencies now becomes clear as the transition fields contain zeta functions of the form $\zeta(\omega_k \pm \omega)$ where the Green's function around $\boldsymbol{\Gamma}_{k_0}(\boldsymbol{R})$ matters. The static contributions, however, contain a zeta function of the form $\zeta(\omega_k)$ where $\boldsymbol{\Gamma}_{k=0}(\boldsymbol{R})$ matters. Since the zeta function essentially only evaluates the Kramers-Kronig relations for the complex function $\boldsymbol{G}(\boldsymbol{R})$, i.e., $(k'^2)\Omega_{k'}(\boldsymbol{R}) = \int dk\frac{k^2\Gamma_k(\boldsymbol{R})}{\omega'-\omega}$. Ultimately, this leads to the explicit representation of the fields, using

the fact that $\lim_{k\to 0} k^2 G_k(\boldsymbol{R}) = \frac{1}{4\pi R_{ij}^3}(3\frac{\boldsymbol{R}_{ij}\boldsymbol{R}_{ij}}{R_{ij}R_{ij}} - 1)$ so that only the real part remains

$$\hat{\boldsymbol{E}}(\boldsymbol{R}_i) = \hat{\boldsymbol{E}}_0(\boldsymbol{R}_i) + \frac{k_0^2}{\epsilon_0}\sum_j [(\boldsymbol{\Gamma}(\boldsymbol{R}_{ij}) - \mathrm{i}\boldsymbol{\Omega}(\boldsymbol{R}_{ij}))\sigma_j + (\boldsymbol{\Gamma}(\boldsymbol{R}_{ij}) + \mathrm{i}\boldsymbol{\Omega}(\boldsymbol{R}_{ij}))\sigma_j^\dagger]\cdot\boldsymbol{d},$$

$$\hat{\boldsymbol{B}}(\boldsymbol{R}_i) = \hat{\boldsymbol{B}}_0(\boldsymbol{R}_i) + \frac{k_0^2}{\epsilon_0}\sum_j [(\boldsymbol{\Gamma}(\boldsymbol{R}_{ij}) - \mathrm{i}\boldsymbol{\Omega}(\boldsymbol{R}_{ij}))\sigma_j + (\boldsymbol{\Gamma}(\boldsymbol{R}_{ij}) + \mathrm{i}\boldsymbol{\Omega}(\boldsymbol{R}_{ij}))\sigma_j^\dagger]\cdot\boldsymbol{\mu}_t,$$

$$\hat{\boldsymbol{B}}_s(\boldsymbol{R}_i) = \frac{\mu_0}{4\pi}\sum_j \frac{1}{R_{ij}^3}\left(3\frac{\boldsymbol{R}_{ij}\boldsymbol{R}_{ij}}{R_{ij}R_{ij}} - 1\right)\cdot\hat{\boldsymbol{\mu}}_{s,j}. \tag{E13}$$

The next step is to plug these expressions into the equations of motion, to use the rotating wave approximation and the definitions $\Gamma = k_0^3 d^2/(3\pi\hbar\epsilon_0)$ and $\Gamma_\mu = k_0^3\mu^2/3\pi\hbar\epsilon_0$ to define the Green's function for the matter problem. Indeed, the definitions

$$f_{ij}^{(\mu)} + \mathrm{i}g_{ij}^{(\mu)} = \frac{3\Gamma_\nu}{4}\left[\left(\frac{k^2}{R_{ij}} + \frac{\mathrm{i}k}{R_{ij}^2} - \frac{1}{R_{ij}^3}\right)\hat{\mu}_i\cdot\hat{\mu}_j + \left(-\frac{k^2}{R_{ij}} - \frac{3\mathrm{i}k}{R_{ij}^2} + \frac{3}{R_{ij}^3}\right)\frac{(\hat{\mu}_j\cdot\mathbf{R}_{ij})(\hat{\mu}_i\cdot\mathbf{R}_{ij})}{R_{ij}^2}\right]\frac{e^{\mathrm{i}kR_{ij}}}{k^2},$$

$$f_{ij}^{(g)} + \mathrm{i}g_{ij}^{(g)} = \frac{3\Gamma}{4}\left[\left(\frac{k^2}{R_{ij}} + \frac{\mathrm{i}k}{R_{ij}^2} - \frac{1}{R_{ij}^3}\right)\hat{d}_i\cdot\hat{d}_j + \left(-\frac{k^2}{R_{ij}} - \frac{3\mathrm{i}k}{R_{ij}^2} + \frac{3}{R_{ij}^3}\right)\frac{(\hat{d}_j\cdot\mathbf{R}_{ij})(\hat{d}_i\cdot\mathbf{R}_{ij})}{R_{ij}^2}\right]\frac{e^{\mathrm{i}kR_{ij}}}{k^2}, \tag{E14}$$

and Eq. (13) lead precisely to Eqs. (12), (14), and (15) after using the rotating wave approximation.

After adding a classical drive just as in the main text, the equations of motion for the transition operators become

$$\frac{d\sigma_k}{dt} = -\mathrm{i}[\Delta + \delta\hat{\omega}_k]\sigma_k + \mathrm{i}\sigma_k^z\sum_{i\neq k}\left(g_{ki}^{(d)} + g_{ki}^{(\mu)}\right)\sigma_i + \sigma_k^z\sum_i\left(f_{ki}^{(d)} + f_{ki}^{(\mu)}\right)\sigma_i - \mathrm{i}\Omega e^{\mathrm{i}\boldsymbol{k}_0\boldsymbol{R}_i}\sigma_k^z + \sigma_{k,\mathrm{in}}, \tag{E15}$$

where $\sigma_{k,\mathrm{in}}$ is the canonical input noise due to spontaneous emission of an atom

$$\sigma_{k,\mathrm{in}} = \mathrm{i}\sigma_k^z\boldsymbol{d}\cdot\boldsymbol{E}_0^+(\boldsymbol{r}_k), \tag{E16}$$

with expectation value zero and a frequency operator

$$\delta\hat{\omega}_k = \frac{1}{2}\sum_{i\neq k}\left[\left(\Omega_{ik}^{e,e} - \Omega_{ik}^{g,g}\right) + \left(\Omega_{ik}^{e,e} + \Omega_{ik}^{g,g} - 2\Omega_{ik}^{e,g}\right)\sigma_i^z\right]. \tag{E17}$$

This is a configuration and density-dependent Zeeman shift of the kth atom's frequency.

APPENDIX F: WEAK-EXCITATION LIMIT

The weak-excitation limit, i.e., $\langle\sigma_j^z\sigma_{j'}\rangle \approx -\langle\sigma_{j'}\rangle$, the equations of motion for the expectation values of the transition operators become

$$\frac{d\langle\sigma_k\rangle}{dt} = -\mathrm{i}[\Delta + \delta\omega_k]\langle\sigma_k\rangle - \mathrm{i}\sum_{i\neq k}\left(g_{ki}^{(d)} + g_{ki}^{(\mu)}\right)\langle\sigma_i\rangle - \sum_i\left(f_{ki}^{(d)} + f_{ki}^{(\mu)}\right)\langle\sigma_i\rangle + \mathrm{i}\Omega e^{\mathrm{i}\boldsymbol{k}_0\boldsymbol{R}_i}, \tag{F1}$$

which is written in matrix notation in Eq. (16).

[1] M. Reitz, C. Sommer, and C. Genes, Cooperative quantum phenomena in light-matter platforms, PRX Quantum **3**, 010201 (2022).

[2] G. Labeyrie, F. de Tomasi, J.-C. Bernard, C. A. Müller, C. Miniatura, and R. Kaiser, Coherent backscattering of light by cold atoms, Phys. Rev. Lett. **83**, 5266 (1999).

[3] G. Labeyrie, D. Delande, C. A. Müller, C. Miniatura, and R. Kaiser, Coherent backscattering of light by an inhomogeneous cloud of cold atoms, Phys. Rev. A **67**, 033814 (2003).

[4] R. H. Dicke, Coherence in spontaneous radiation processes, Phys. Rev. **93**, 99 (1954).

[5] M. Gross and S. Haroche, Superradiance: An essay on the theory of collective spontaneous emission, Phys. Rep. **93**, 301 (1982).

[6] W. Guerin, M. O. Araújo, and R. Kaiser, Subradiance in a large cloud of cold atoms, Phys. Rev. Lett. **116**, 083601 (2016).

[7] M. O. Araújo, I. Krešić, R. Kaiser, and W. Guerin, Superradiance in a large and dilute cloud of cold atoms in the linear-optics regime, Phys. Rev. Lett. **117**, 073002 (2016).

[8] J. Keaveney, A. Sargsyan, U. Krohn, I. G. Hughes, D. Sarkisyan, and C. S. Adams, Cooperative Lamb shift in an atomic vapor layer of nanometer thickness, Phys. Rev. Lett. **108**, 173601 (2012).

[9] J. Javanainen, J. Ruostekoski, Y. Li, and S.-M. Yoo, Shifts of a resonance line in a dense atomic sample, Phys. Rev. Lett. **112**, 113603 (2014).

[10] S. D. Jenkins, J. Ruostekoski, J. Javanainen, R. Bourgain, S. Jennewein, Y. R. P. Sortais, and A. Browaeys, Optical resonance shifts in the fluorescence of thermal and cold atomic gases, Phys. Rev. Lett. **116**, 183601 (2016).

[11] J. Javanainen and J. Ruostekoski, Light propagation beyond the mean-field theory of standard optics, Opt. Express **24**, 993 (2016).

[12] M. O. Scully, E. S. Fry, C. H. R. Ooi, and K. Wódkiewicz, Directed spontaneous emission from an extended ensemble of *N* atoms: Timing is everything, Phys. Rev. Lett. **96**, 010501 (2006).
[13] P. Weiss, A. Cipris, M. O. Araújo, R. Kaiser, and W. Guerin, Robustness of Dicke subradiance against thermal decoherence, Phys. Rev. A **100**, 033833 (2019).
[14] R. Kaiser, Quantum multiple scattering, J. Mod. Opt. **56**, 2082 (2009).
[15] R. A. de Oliveira, M. S. Mendes, W. S. Martins, P. L. Saldanha, J. W. R. Tabosa, and D. Felinto, Single-photon superradiance in cold atoms, Phys. Rev. A **90**, 023848 (2014).
[16] S. J. Roof, K. J. Kemp, M. D. Havey, and I. M. Sokolov, Observation of single-photon superradiance and the cooperative Lamb shift in an extended sample of cold atoms, Phys. Rev. Lett. **117**, 073003 (2016).
[17] C. C. Kwong, T. Yang, D. Delande, R. Pierrat, and D. Wilkowski, Cooperative emission of a pulse train in an optically thick scattering medium, Phys. Rev. Lett. **115**, 223601 (2015).
[18] B. Zhu, J. Cooper, J. Ye, and A. M. Rey, Light scattering from dense cold atomic media, Phys. Rev. A **94**, 023612 (2016).
[19] S. L. Bromley, B. Zhu, M. Bishof, X. Zhang, T. Bothwell, J. Schachenmayer, T. L. Nicholson, R. Kaiser, S. F. Yelin, M. D. Lukin, A. M. Rey, and J. Ye, Collective atomic scattering and motional effects in a dense coherent medium, Nat. Commun. **7**, 11039 (2016).
[20] S. Jennewein, L. Brossard, Y. R. P. Sortais, A. Browaeys, P. Cheinet, J. Robert, and P. Pillet, Coherent scattering of near-resonant light by a dense, microscopic cloud of cold two-level atoms: Experiment versus theory, Phys. Rev. A **97**, 053816 (2018).
[21] A. A. Svidzinsky, J.-T. Chang, and M. O. Scully, Cooperative spontaneous emission of *N* atoms: Many-body eigenstates, the effect of virtual Lamb shift processes, and analogy with radiation of *N* classical oscillators, Phys. Rev. A **81**, 053821 (2010).
[22] M. Lewenstein, L. You, J. Cooper, and K. Burnett, Quantum field theory of atoms interacting with photons: Foundations, Phys. Rev. A **50**, 2207 (1994).
[23] J. Ruostekoski and J. Javanainen, Quantum field theory of cooperative atom response: Low light intensity, Phys. Rev. A **55**, 513 (1997).
[24] J. Javanainen, J. Ruostekoski, B. Vestergaard, and M. R. Francis, One-dimensional modeling of light propagation in dense and degenerate samples, Phys. Rev. A **59**, 649 (1999).
[25] M. D. Lee, S. D. Jenkins, and J. Ruostekoski, Stochastic methods for light propagation and recurrent scattering in saturated and nonsaturated atomic ensembles, Phys. Rev. A **93**, 063803 (2016).
[26] T. Busch, J. R. Anglin, J. I. Cirac, and P. Zoller, Inhibition of spontaneous emission in Fermi gases, Europhys. Lett. **44**, 1 (1998).
[27] B. DeMarco and D. S. Jin, Exploring a quantum degenerate gas of fermionic atoms, Phys. Rev. A **58**, R4267 (1998).
[28] J. Ruostekoski and J. Javanainen, Optical linewidth of a low density Fermi-Dirac gas, Phys. Rev. Lett. **82**, 4741 (1999).
[29] T. Bilitewski, A. P. Orioli, C. Sanner, L. Sonderhouse, R. B. Hutson, L. Yan, W. R. Milner, J. Ye, and A. M. Rey, Disentangling Pauli blocking of atomic decay from cooperative radiation and atomic motion in a 2D Fermi gas, Phys. Rev. Lett. **128**, 093001 (2022).
[30] A. Görlitz, A. P. Chikkatur, and W. Ketterle, Enhancement and suppression of spontaneous emission and light scattering by quantum degeneracy, Phys. Rev. A **63**, 041601(R) (2001).
[31] S. Inouye, A. P. Chikkatur, D. M. Stamper-Kurn, J. Stenger, D. E. Pritchard, and W. Ketterle, Superradiant Rayleigh scattering from a Bose-Einstein condensate, Science **285**, 571 (1999).
[32] W. J. Childs, Hyperfine structure of $^5I_{8,7}$ atomic states of $Dy^{161,163}$ and the ground-state nuclear moments, Phys. Rev. A **2**, 1692 (1970).
[33] N. Petersen, M. Trümper, and P. Windpassinger, Spectroscopy of the 1001-nm transition in atomic dysprosium, Phys. Rev. A **101**, 042502 (2020).
[34] D. F. V. James, Frequency shifts in spontaneous emission from two interacting atoms, Phys. Rev. A **47**, 1336 (1993).
[35] R. H. Lehmberg, Radiation from an *N*-atom system. I. general formalism, Phys. Rev. A **2**, 883 (1970).
[36] W. Guerin, T. S. do Espirito Santo, P. Weiss, A. Cipris, J. Schachenmayer, R. Kaiser, and R. Bachelard, Collective multimode vacuum Rabi splitting, Phys. Rev. Lett. **123**, 243401 (2019).
[37] F. Mühlbauer, N. Petersen, C. Baumgärtner, L. Maske, and P. Windpassinger, Systematic optimization of laser cooling of dysprosium, Appl. Phys. B **124**, 120 (2018).
[38] M. Lu, N. Q. Burdick, S. H. Youn, and B. L. Lev, Strongly dipolar Bose-Einstein condensate of dysprosium, Phys. Rev. Lett. **107**, 190401 (2011).
[39] M. Lu, N. Q. Burdick, and B. L. Lev, Quantum degenerate dipolar Fermi gas, Phys. Rev. Lett. **108**, 215301 (2012).
[40] A. Frisch, K. Aikawa, M. Mark, A. Rietzler, J. Schindler, E. Zupanič, R. Grimm, and F. Ferlaino, Narrow-line magneto-optical trap for erbium, Phys. Rev. A **85**, 051401(R) (2012).
[41] T. Maier, H. Kadau, M. Schmitt, A. Griesmaier, and T. Pfau, Narrow-line magneto-optical trap for dysprosium atoms, Opt. Lett. **39**, 3138 (2014).
[42] T. L. Gustavson, A. P. Chikkatur, A. E. Leanhardt, A. Görlitz, S. Gupta, D. E. Pritchard, and W. Ketterle, Transport of Bose-Einstein condensates with optical tweezers, Phys. Rev. Lett. **88**, 020401 (2001).
[43] W. Alt, An objective lens for efficient fluorescence detection of single atoms, Optik **113**, 142 (2002).
[44] X. Li, F. Zhou, M. Ke, P. Xu, X.-D. He, J. Wang, and M.-S. Zhan, High-resolution *ex vacuo* objective for cold atom experiments, Appl. Opt. **57**, 7584 (2018).